Available online at www.sciencedirect.com
ScienceDirect
Catalysis Today 125 (2007) 111–119
CATALYSIS TODAY
www.elsevier.com/locate/cattod

# Catalytic dehydration of bioethanol to ethylene over $TiO_2/\gamma$-$Al_2O_3$ catalysts in microchannel reactors

Guangwen Chen *, Shulian Li, Fengjun Jiao, Quan Yuan

*Dalian Institute of Chemical Physics, Chinese Academy of Sciences, 457 Zhongshan Road, Dalian 116023, China*

Available online 21 March 2007

**Abstract**

Ethylene is essential material for the petrochemical industry. Ethylene production via catalytic dehydration of ethanol over $TiO_2/\gamma$-$Al_2O_3$ catalysts in multi-microchannel reactors is reported in this paper. The physicochemical properties of these catalysts are characterized by X-ray diffraction (XRD) and FT-IR spectrum. The effects of operation parameters, such as ethanol concentration, reaction temperature and liquid hourly space velocity, have been investigated experimentally. The reaction results indicate that the catalysts doped with $TiO_2$ have high ethanol conversion of 99.96% and ethylene selectivity of 99.4%. Ethylene yield of 26 g/($g_{cat}$ h) can be achieved, which provides very favorable foundation for the process intensification and miniaturization of the ethylene production process using bioethanol.


*Keywords:* Ethanol dehydration; Ethylene; Ti/$\gamma$-$Al_2O_3$ catalyst; Microchannel; Microstructured reactor; Microreactor; Miniaturization; Process intensification

## 1. Introduction

Ethylene is crucial material for the petrochemical industry, which is derived mainly from steam-cracking of petroleum or natural gas feedstocks. Due to the high production cost and high energy consumption, the way of ethanol catalytic dehydration into ethylene is commercially applied only in a few countries, such as Brazil and India. Nowadays, with the shortage of natural resource and energy, and also with the skyrocketing prices of crude oil, catalytic dehydration of ethanol (especially bioethanol) to ethylene has become a more and more competitive and promising route, and therefore has been drawing much attention.

For catalytic reactions, development of an effective catalyst is the foundational and critical step. Many catalysts have been studied for ethylene production via ethanol dehydration process. These catalysts are mainly pure or doped alumina [1–4]; the rest are zeolite [5], titania–silica [6], magnesium oxides [7], manganese oxides [8,9], cobalt oxides [10], chromium oxide [11], zirconium phosphite [12], silver salt of tungstophosphoric acid [13], etc. Dopants for alumina based catalysts that have been studied are mostly transition metals. Phillips Oil Co. [1,2] reported the application of $\gamma$-$Al_2O_3$ catalyst treated with KOH and $ZnO/Al_2O_3$ catalyst for the dehydration of saturated alcohol to produce the corresponding olefin. Syndol catalyst based on $MgO–Al_2O_3/SiO_2$ developed by Halcon SD has been applied commercially [3]. El-Katatny et al. [14] developed $FeO_x/\gamma$-$Al_2O_3$ catalyst, but ethanol conversion and ethylene selectivity were only 60% and 68% at temperature of 250 °C, respectively. Doheim et al. [15] developed $Na_2O$-doped $Mn_2O_3/Al_2O_3$ catalyst, and as high as 97% ethanol conversion could be achieved at 300 °C and a low space velocity. The reactors used in industry are usually the tube-array fixed bed reactors with low liquid hourly space velocity (0.3–0.6 $h^{-1}$), low ethylene yield, and relatively high reaction temperature (350–450 °C), resulting in high energy consumption and low utilization of equipment capacity.

Two reactions can occur in parallel during catalytic dehydration of ethanol:

$$C_2H_5OH = C_2H_4 + H_2O \quad +44.9\,kJ/mol \tag{1}$$

$$2C_2H_5OH = C_2H_5OC_2H_5 + H_2O \quad -25.1\,kJ/mol \tag{2}$$

The main reaction and the side reaction are endothermic and exothermic, respectively. Low temperatures favor the side reaction, so how to enhance the reactor performance and how to keep the isothermal operation are key issues of this process to achieve high efficiencies.

* Corresponding author. Tel.: +86 411 84379031; fax: +86 411 84691570.
*E-mail address:* gwchen@dicp.ac.cn (G. Chen).

0920-5861/$ – see front matter © 2007 Elsevier B.V. All rights reserved.
doi:10.1016/j.cattod.2007.01.071

With the great progresses achieved in the new area of microreactor technologies [16–18], microreactors have been widely applied in the field of heterogeneous catalytic reactions, including catalytic hydrogenations/dehydrogenations [19], ammonia oxidation [20], hydrogen combustion [21], fuel reforming [22–24], selective oxidation of hydrocarbons [25–27], etc. Microchannel reactors usually refer to miniaturized reaction systems fabricated by methods of microtechnology and precision engineering; their characteristic dimensions of the internal structures range from dozen micrometers to sub-millimeters. When applied in chemical reactions, microreactors possess many fundamental advantages and can bring many benefits that cannot be achieved in traditional reactors. These advantages include decreased physical sizes, increased surface-to-volume ratios, excellent mass and heat transfer capabilities, better process safety, high yields, and facility for easily scaling up and production on site, etc. The application of microreaction technology can improve the efficiency of systems and diminish their volumes and weights.

In order to fulfill the process intensification of ethanol catalytic dehydration to ethylene, and thus to enhance the economic benefit and competence of this process over the petroleum steam-cracking processes, both the catalysts with high activities and novel reactors need to be developed. Three main ways were applied for catalyst immobilization in microchannel, the one is that the reactors or microchannels themselves were made of active materials, the two others are wall-coating technique and catalysts packed into channels in the form of powder, small pellets or structured strips [28]. In this work, we aim at investigating the modification effects of $TiO_2$-doped on alumina catalysts packed in microreactors. The catalysts modified are compared with the undoped one in reaction performance. After choosing an appropriate catalyst and optimal reaction conditions, higher yield of ethylene can be obtained.

## 2. Experimental

### 2.1. Microreactor design

The configuration of the microchannel reactor used in the experiments is shown in Fig. 1. A stainless steel chip of the microreactor is made by microprecision-machining method. Thirty microchannels per chip are separated by 500 μm fins; its width, depth and length are 1000 μm, 1250 μm and 30 mm, respectively. The entrance and exit areas are triangular shaped with the inlets and outlets on opposite sides of the channels array. Catalyst particles with the size of 40–60 mesh are packed within the 30 parallel channels. Quartz wool is set at each end of the catalysts to keep them from moving with the stream flow. A graphite sheet covers the plate to seal the channels. The total volume of the channels packed with catalyst is about 1.15 mL.

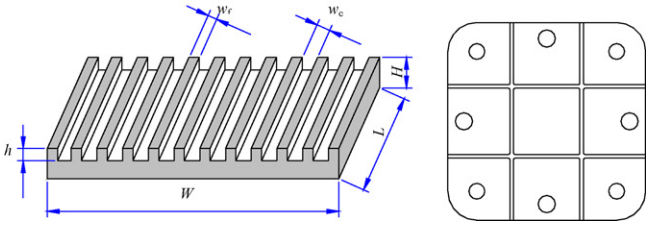


Fig. 1. Microchannel reactor configuration. *W*, width of total channels 44.5 mm; $w_c$, width of single channel 1.0 mm; $w_f$, width of fin 0.5 mm; *h*, depth of channel 1.25 mm; *H*, thickness of chip 2 mm; *L*, length of channel 30 mm.

Four grooves are made across in the back of the plate, where a thermocouple can be inserted and moved smoothly to control or measure the temperature of different regions of the reaction plate. The plate is firmly sandwiched between two stainless steel housings, which integrate four columnar heaters, a thermocouple, the inlet and the outlet. The heaters are inserted into both the top and bottom plates to keep the channels of the reaction plate at a certain temperature. Stainless bolts are used to hold all the parts.

### 2.2. Experimental set-up

The reaction of ethanol catalytic dehydration to ethylene is carried out in a microchannel reactor at the atmospheric pressure. Through a micro liquid pump with precision of 0.001 mL/min, the mixture of ethanol and water with different compositions is pumped into a vaporizer kept at 200 °C and conveys into the microreactor. The reaction temperature inside the microreactor is controlled at the range of 300–500 °C, the liquid hourly space velocity (LHSV) based on volume of ethanol and water mixture is kept at 26–234 $h^{-1}$, and the weight concentration of ethanol is kept at 12–100 wt%. The products are condensed via a cold trap with a mixture of ice and water; both the gas and the liquid phase products are analyzed by a GC (GC-960, Shanghai Haixin GC Co.) using 406-organic-carrier column, $H_2$ as carrier gas and TCD detector at an oven temperature of 120 °C.

### 2.3. Gas analysis and calculation

Gas phase products consist of a large amount of ethylene (E), a small amount of diethyl ether (DEE) and ethanol (EtOH), and a trace amount of ethane, propane, propylene, *iso*-butane, *normal*-butane and *iso*-pentane as well. In liquid phase, a large amount is water and the rest is ethanol and DEE. In order to eliminate the errors caused by the GC analysis, the data of each reaction condition are obtained by repeating the measurement two or three times.

In this paper, the liquid hourly space velocity is defined as the ratio of the hourly feed volumetric flow rate of ethanol and water mixture to the catalyst volume (1.15 mL). The ethanol conversion ($X_{MeOH}$), the ethylene selectivity ($S_E$) and the diethyl ether selectivity ($S_{DEE}$) are defined as the following:

$$X_{EtOH} = \frac{n_{EtOH,0} - n_{EtOH,1}}{n_{EtOH,0}} \times 100 \quad (3)$$

$$S_E = \frac{n_{E,1}}{\sum n_{i,1}} \times 100 \quad (4)$$

$$S_{DEE} = \frac{2n_{DEE,1}}{\sum n_{i,1}} \times 100 \quad (5)$$

where $n_{EtOH,0}$ and $n_{EtOH,1}$ are defined as the molar flow rate (mmol/min) of ethanol in feed and in products, respectively; $n_{E,1}$, $n_{DEE,1}$, and $\sum n_{i,1}$ are defined as the molar flow rate of ethylene, diethyl ether and total products, respectively.

### 2.4. Catalyst preparation

The procedure to prepare the $TiO_2/\gamma$-$Al_2O_3$ catalysts is described as the following steps. Firstly, 30 g $\gamma$-$Al_2O_3$ powder with BET specific surface areas of 200 $m^2/g$ are diluted and mixed well with a small quantity of 0.5 mol/L $Na_2CO_3$ solution in a three-necked rounded-bottomed flask. Then, 0.19 mol/L $Ti(SO_4)_2$ aqueous solution and 0.5 mol/L $Na_2CO_3$ solution are added simultaneously to the flask, and agitate well with a magnetic stirrer. Keep the pH of the solution at 7–8, and then the material is washed to eliminate $SO_4^{2-}$ via a centrifugal machine, followed by dried at 110 °C for 8 h and calcined at 500 °C for 4 h. Finally, the $TiO_2/\gamma$-$Al_2O_3$ catalysts with the size of 30–50 mesh are obtained after forming, crushing and sieving.

### 2.5. Catalyst characterization

The catalyst powders are examined by X-ray diffraction (XRD) for the phase identification. The determination of the crystallinity is performed on an X'pert PRO diffractometer (PANalytical Inc.) equipped with Cu Kα radiation with an accelerating voltage of 40 kV and current of 40 mA. The patterns are recorded over the $2\theta$ angle ranging from 10° to 70° at a scan rate of 4°/min.

The acidity and its distribution are analyzed by $NH_3$ adsorption and $NH_3$-TPD. 0.1 g catalyst sample is heated for 2 h at 450 °C under helium with flow rate of 40 mL/min, and then at 100 °C for impulse $NH_3$ adsorption. When saturated adsorption is achieved, the system is swept by He for 15 min. Then, temperature is programmed to increase to 400 °C under the heating up rate of 15 °C/min.

Surface acid types of catalysts are investigated by pyridine FT-IR. The adsorbed state of pyridine is measured using EQUINOX55 FT-IR (Bruker Instrument Corporation). IR cell is connected to the high-vacuum system, and the temperature of the cell is controlled by a temperature programmer. The dried catalyst powder for measurement is well ground and pressed into wafers with a 16 mg/$cm^2$ density before setting into the IR adsorption cell. All the samples used are desiccated under 450 °C and a vacuum pressure of $0.7 \times 10^{-3}$ Pa for 4 h in order to remove the physically adsorbed water. To study the static behavior of the catalysts at deferent evacuation temperatures, the pyridine desorption under vacuum conditions is carried out to observe the change of pyridine spectra in the process. At first, pyridine is adsorbed at room temperature by the pretreated catalysts and kept for 5 min, then the pyridine in the system is drawn out after vacuumizing for 6 h at different temperatures while the system maintained vacuum. A computer is used to record the IR spectra synchronously during the process.

The specific surface areas and the pore distribution of the catalysts are determined by the nitrogen physisorption using the BET method in ASAP2010 instruments (Micromeritics Instrument Corporation, USA).

## 3. Results and discussion

### 3.1. Structure and crystal phase

As shown in Fig. 2, the $N_2$ adsorption–desorption isotherms of the catalysts at the liquid nitrogen temperature (−196 °C) are found to have reversible isotherms exhibiting close hysteresis loops of type II. The values of the specific surface areas ($A_{BET}$), the pore volume ($V_P$) and the pore radius ($r_P$) are listed in Table 1, calculated by the BJH method. From Fig. 2 and Table 1, we can see that both of the $TiO_2$-doped $Al_2O_3$ and pure $Al_2O_3$ catalyst have similar pore radii and pore size distributions, and both catalysts are mesoporous in nature. The surface area and the pore volume of the $TiO_2$-doped $Al_2O_3$ catalysts have a small decrease compared with pure $Al_2O_3$. It can affect the $A_{BET}$ and $V_P$ of catalysts when $TiO_2$ deposited on the surface or penetrated into the body phase of $Al_2O_3$ due to the mixing of alumina with low-surface-area $TiO_2$.

Fig. 3 shows the XRD patterns of different $TiO_2/Al_2O_3$ samples calcined at 500 °C for 4 h. Diffraction characteristic peaks of pure $TiO_2$ and the crystal phase of new species cannot be observed by XRD in the samples when dopant $TiO_2$ concentration is less than 10 wt%. It suggests that $TiO_2$ is uniformly dispersed on the surface or intruded into the body phase of $Al_2O_3$, thus resulting in decrement of the specific surface area of the doped catalysts. However, characteristic

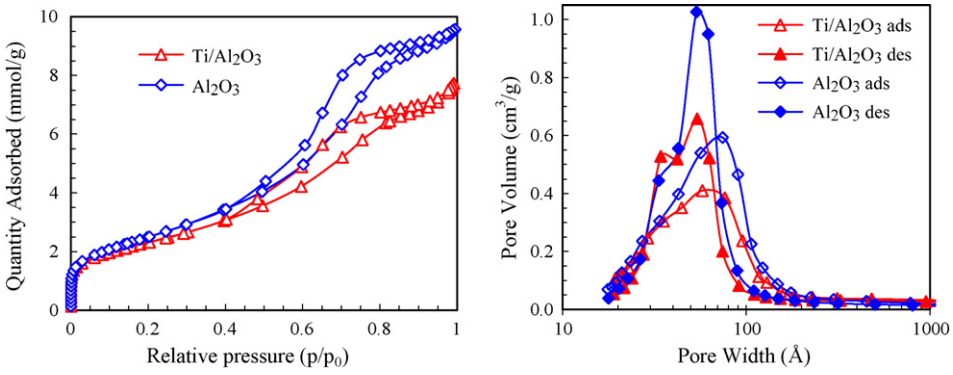


Fig. 2. $N_2$ adsorption–desorption isotherms and BJH pore volume of $Al_2O_3$ and $TiO_2/Al_2O_3$.

Table 1
Specific surface area and pore structure of different catalysts

| Sample | $TiO_2$ (wt%) | $A_{BET}$ ($m^2$/g) | $V_P$ ($cm^3$/g) | $r_P$ (Å) |
|---|---|---|---|---|
| $Al_2O_3$ | 0 | 204.1 | 0.341 | 53.4 |
| $TiO_2/Al_2O_3$ | 10 | 186.9 | 0.278 | 53.8 |

peaks at Bragg angle $2\theta$ of 25.73° ascribed to the crystal phase of $TiO_2$ in anatase can be detected in XRD patterns when the $TiO_2$ concentration is higher than 20 wt%, suggesting that the amount of dopant exceeds the largest capacity of the single layer distribution on the $Al_2O_3$ surface.

### 3.2. Surface acidity of catalysts

Generally, the acid site centers of the solid superstrong acid surface via metal sulfate mainly originates from sulfate ion coordination adsorbed on the surface, resulting in shifting of electron cloud of associated bond between the metal and oxygen atoms, and the increment of the L-acid centers. In order to investigate the surface acidity of $TiO_2/Al_2O_3$ catalysts prepared in the previous section, the methods of FT-IR spectrum with pyridine adsorption and $NH_3$-TPD are adopted to characterize the acidity and its distribution across the catalysts.

The infrared spectra of pyridine static adsorbed on $TiO_2/Al_2O_3$ at room temperature and desorbed at different temperatures are shown in Fig. 4. The FT-IR results reveal that the acid types on both the pure $Al_2O_3$ and $TiO_2$-doped $Al_2O_3$ from pyridine adsorption IR are identical [29], due to the pyridine adsorb onto the Lewis acid centers on the solid surface with a covalent bond. After evacuations at 150 and 450 °C, the persistence and frequency shifting of spectrum band of 1450 and 1610 $cm^{-1}$ indicates that $TiO_2$-doped $Al_2O_3$ is still Lewis acid. Adsorbance of residual pyridine reflects the intensity of Lewis acid center after desorption at different evacuation temperatures. The larger adsorbance, the higher intensity. From Fig. 4, the acidity of 10 wt% $TiO_2/Al_2O_3$ is strong, and maintains more Lewis acid centers after desorption at an evacuation temperature of 450 °C, indicating that $TiO_2$ content affects the acidity of the catalysts.

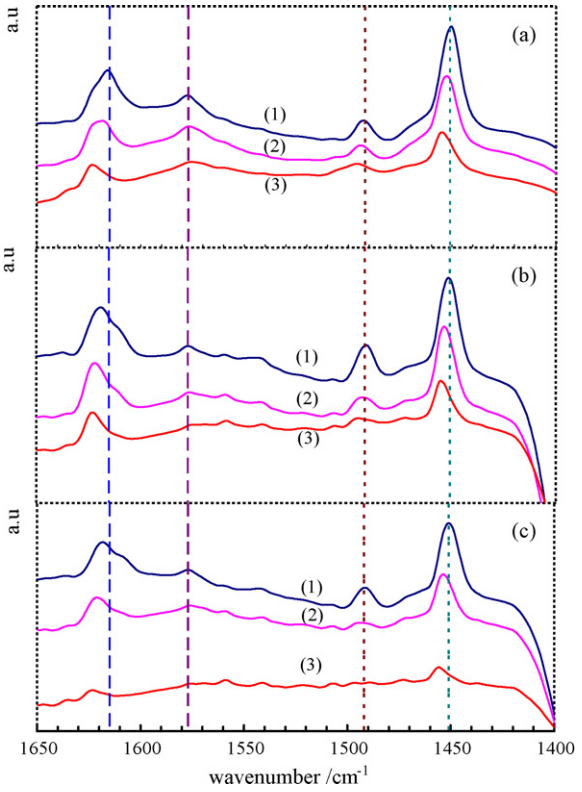


Fig. 4. Infrared spectra of pyridine static adsorbed on $TiO_2/Al_2O_3$ at room temperature. $TiO_2$ (wt%): (a) 5.0, (b) 10.0, and (c) 20.0. Evacuation temperature: (1) 150 °C, (2) 300 °C, and (3) 450 °C.

Based on the adsorption peak intensities at evacuation temperature of 150 °C, normalized adsorption peak intensities at 1450 $cm^{-1}$ and different evacuation temperatures are shown in Fig. 5. The results indicate that the adsorption peak intensity decreases with increasing evacuation temperatures, and also show the strongest acidity in the sample of 10 wt% $TiO_2/Al_2O_3$, while the lowest acidity is observed in 20 wt% $TiO_2/Al_2O_3$ catalyst where part of $TiO_2$ dissociated from the surface of

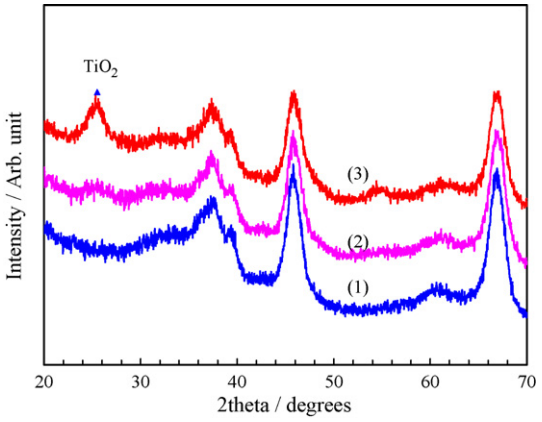


Fig. 3. XRD patterns of different $TiO_2/Al_2O_3$ samples calcined at 500 °C for 4 h. $TiO_2$ (wt%): (1) 0, (2) 10, and (3) 20.

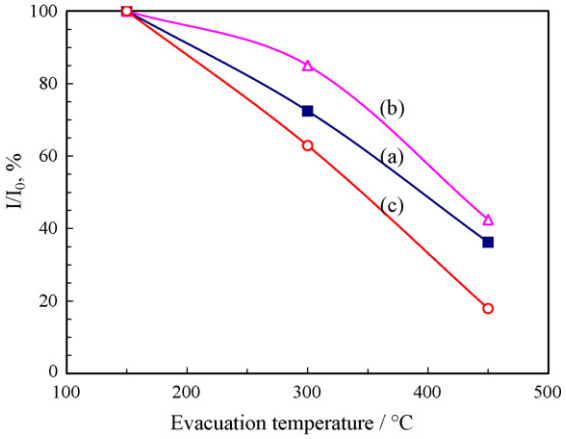


Fig. 5. Normalized adsorption peak intensities at 1450 $cm^{-1}$ at different evacuation temperature. $TiO_2$ (wt%): (a) 5.0, (b) 10.0, and (c) 20.0.

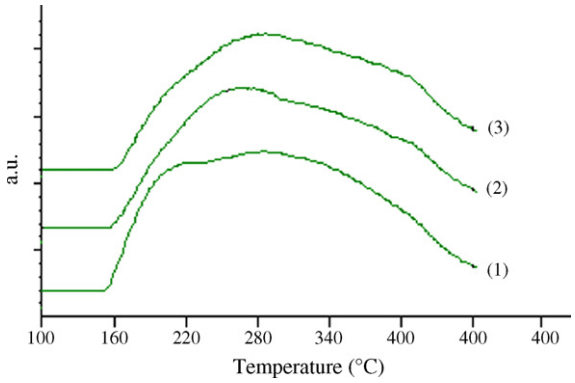


Fig. 6. TPD spectra of ammonia adsorbed on $Al_2O_3$ and $TiO_2/Al_2O_3$: (1) $Al_2O_3$, (2) 10% $TiO_2/Al_2O_3$, and (3) 20% $TiO_2/Al_2O_3$.

$Al_2O_3$ and formed pure crystal phase as also indicated in Fig. 3. The Lewis acidity sites in $TiO_2$ interact with pyridine to form coordinative complex compounds with poor stabilities since there are only weak acidity centers of Hammett $H_0 > 3.3$ in $TiO_2$ [30]. Therefore, the adsorption peaks of 1492 and 1577 $cm^{-1}$ almost disappear, while the peak intensities of 1455 and 1625 $cm^{-1}$ are much weaker than those of 10 wt% $TiO_2/Al_2O_3$. This phenomenon also validate in the results of $NH_3$-TPD shown in Fig. 6.

The dispersed and overlapped desorption spectra of pure $Al_2O_3$ can be clearly observed in Fig. 6, showing that the distribution of surface acidity intensities is nonuniform, and that there exists a desorption peak at the temperature of 200 °C in pure $Al_2O_3$. However, the desorption peak at temperatures below 200 °C has not appeared in $TiO_2$-doped $Al_2O_3$ catalysts (Fig. 6(2) and (3)). The highest temperatures ($T_m$) of desorption peaks in 10 and 20 wt% $TiO_2/Al_2O_3$ are about 260 and 300 °C, respectively. From a qualitative viewpoint, Berteau and Delmon [9] proposed a classification: $T_m$ from 20 to 200 °C is corresponding to the weak acid sites; $T_m$ between 200 and 400 °C is corresponding to moderate acid sites; $T_m$ higher than 400 °C is associated with strong acid sites. According to this classification, the desorption peak at 200 °C in pure $Al_2O_3$ can be ascribed to weak acid sites, and the acid in $TiO_2/Al_2O_3$ can be regarded as moderate acid centers. The catalysts with weak acid centers and moderate acid centers have high activities for the isomerization of paraffins [31]. The catalysts with moderate acid centers have relatively high activities for catalytic dehydration of alcohol, while weak acid centers have no activities [9].

### 3.3. Catalyst activity test

#### 3.3.1. Effect of reaction temperature

As we know, the product distribution of methanol catalytic dehydration depends on reaction temperatures strongly. High reaction temperatures are propitious to the ethylene formation via intra-molecular dehydrations, while low temperatures to diethyl ether via inter-molecular dehydration. At low temperatures, not only the catalyst activity is poor, but also the selectivity of ethylene is low due to a large number of ethanol converted to diethyl ether (Fig. 7). Arai et al. [32] proposed that at low reaction temperatures, the formation of ethyl ether was much easier with increased ethoxyl on the surface of alumina, while the formation of ethylene was controlled by both the concentrations of ethoxyl and hydroxyl on the surface. However, the formation of ethylene is independent of these surface concentrations at high reaction temperatures.

The effects of reaction temperatures on the conversion of ethanol and the selectivities of ethylene and diethyl ether over the catalysts are shown in Fig. 7. The results indicate that the conversion of ethanol and the selectivity of ethylene increase quickly with temperature rising, but the selectivity of diethyl ether is contrary. For γ-$Al_2O_3$, the conversion of ethanol is higher than 90% as the reaction temperature is higher than 460 °C. However, the reaction temperature is lowered by 50 °C at the same conversion for Ti/γ-$Al_2O_3$, and the ethanol conversion is nearly 100% at 460 °C. The selectivity of ethylene is as high as 98.7% in 10 wt% Ti/γ-$Al_2O_3$ which is much higher than that of pure alumina. Both the ethanol conversion and the ethylene selectivity in 10 wt% Ti/γ-$Al_2O_3$ are superior to that of 20 wt% Ti/γ-$Al_2O_3$ to certain extents.

#### 3.3.2. Effect of space velocity

The conversion of ethanol and the selectivities of ethylene and diethyl ether over 10 wt% $TiO_2$/γ-$Al_2O_3$ catalysts are plotted in Fig. 8 as a function of space velocity in the microchannel reactor. The LHSVs in the microreactor vary from 26 to 234 $h^{-1}$. The ethanol concentration in the feed is

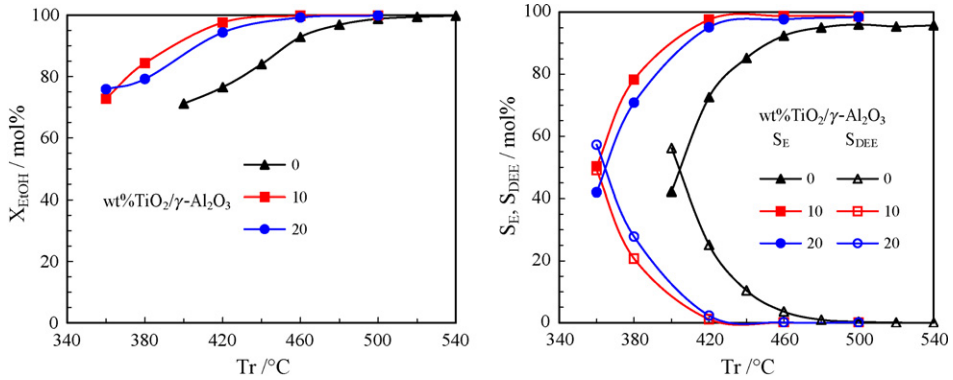


Fig. 7. Effect of reaction temperature on ethanol conversion and selectivities of ethylene and of diethyl ether over three different catalysts filled in microchannel chip. Reaction condition: LHSV = 52 $h^{-1}$; Feed with 100% $C_2H_5OH$ for pure γ-$Al_2O_3$, 93.8 wt% $C_2H_5OH$ for $TiO_2$ doped γ-$Al_2O_3$.

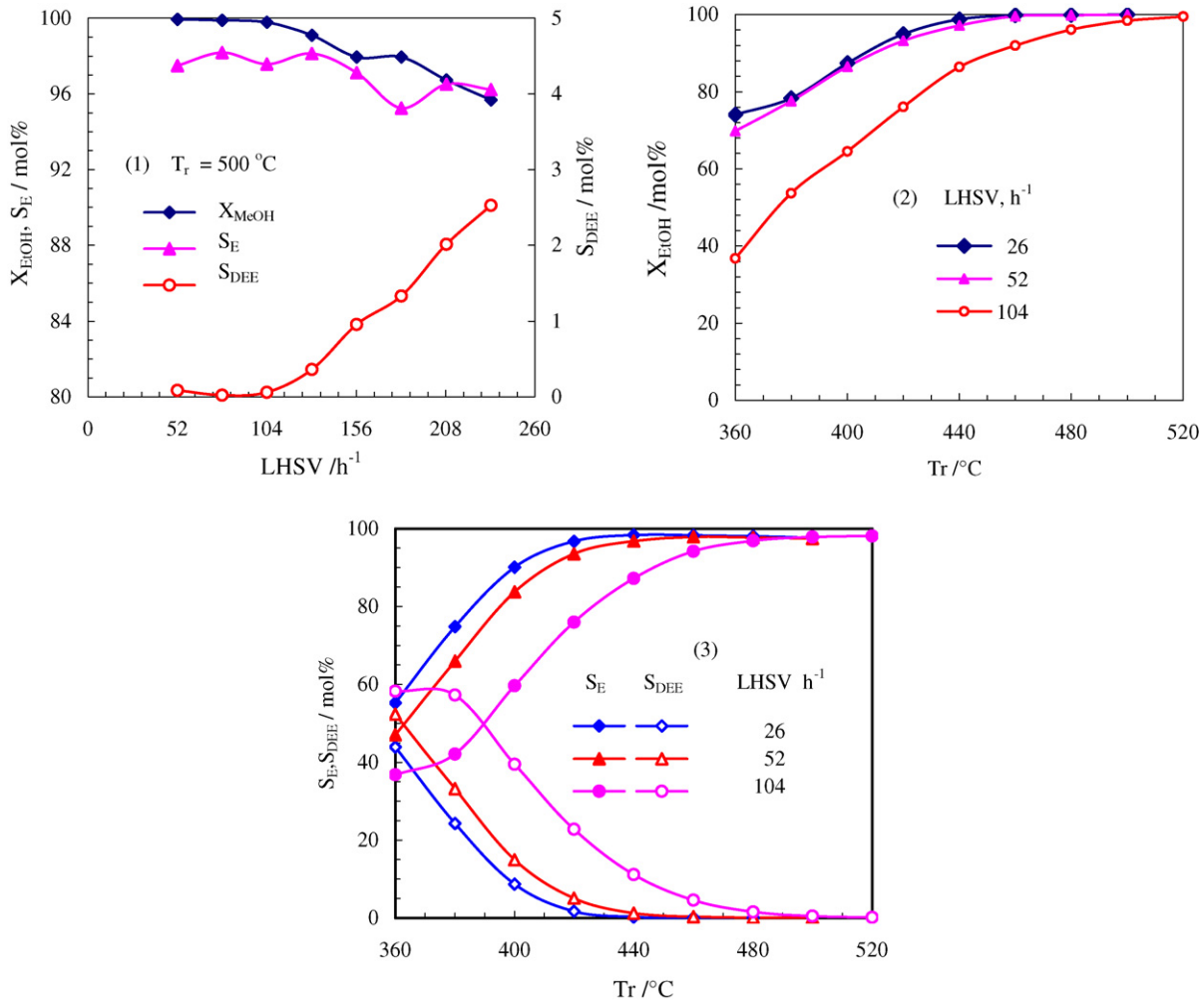


Fig. 8. Ethanol conversion and ethylene and diethyl ether selectivity vs. LHSV and $T_r$ over 10 wt% Ti/γ-$Al_2O_3$ catalyst (93.8 wt% ethanol in feed).

93.8 wt%. The liquid hourly space velocities in the traditional fixed bed reactor are as low as 0.2–0.4 $h^{-1}$ due to the heat transfer and intrinsic reaction rate limitations. Heat and mass transfer is enhanced remarkably with its inherent small dimensions of microreactor, whereas the process is controlled by the reaction rate due to its slow intrinsic reaction rate of ethanol catalytic dehydration to ethylene. High reaction temperatures are needed to enhance the reaction rate at high LHSVs, and finally to achieve the process intensification and process miniaturization purposes.

The results in Fig. 8(1) indicate that the ethanol conversion and the ethylene selectivity decreased with rising space velocities but the selectivity of diethyl ether behaved in the opposite way. The conversion of ethanol is higher than 98% and the selectivity of ethylene is not less than 97%, $S_{DEE} < 1\%$ at the LHSV of 156 $h^{-1}$ and the reaction temperature of 500 °C. Fig. 8(2) and (3) shows that the minimum reaction temperatures are 440, 460 and 480 °C corresponding to the LHSVs of 26, 52 and 104 $h^{-1}$ with the ethanol conversion above 99%, respectively. Under the LHSV of 104 $h^{-1}$, the ethanol conversions are as high as 92% and 96% at the reaction temperatures of 460 and 480 °C, respectively, corresponding to the yields of ethylene of 66.6 and 72.7 $g_{C_2H_4}/(g_{cat}\ h)$. It can be inferred from the results that the microreactor can intensify mass transfer to realize the miniaturization of the bioethanol-to-ethylene process.

Table 2 lists the comparison results between the microreactor and the traditional fixed bed reactor. From this table we can find that for the process of ethanol-to-ethylene, the ethylene yield in the microreaction system is 1–2 orders of magnitude higher than that of the traditional fixed bed reactor.

Table 2
Comparison between the microreactor and traditional fixed bed reactor

| | Reactor | Catalyst | $T_r$ (°C) | WHSV ($h^{-1}$) | $X_{EtOH}$ (mol%) | $S_E$ (mol%) | $Y_E$ (g/(gcat h)) |
|---|---|---|---|---|---|---|---|
| SD Co. | Fixed bed | Syndol | 318–450 | 0.23–1.17 | 97–99 | 94.5–98.9 | 0.22–0.67 |
| This work | Micoreactor | Ti/γ-$Al_2O_3$ | 360–500 | 26–104[a] | 95–99.96 | 96–99.34 | 15–72.7 |

[a] LHSV.

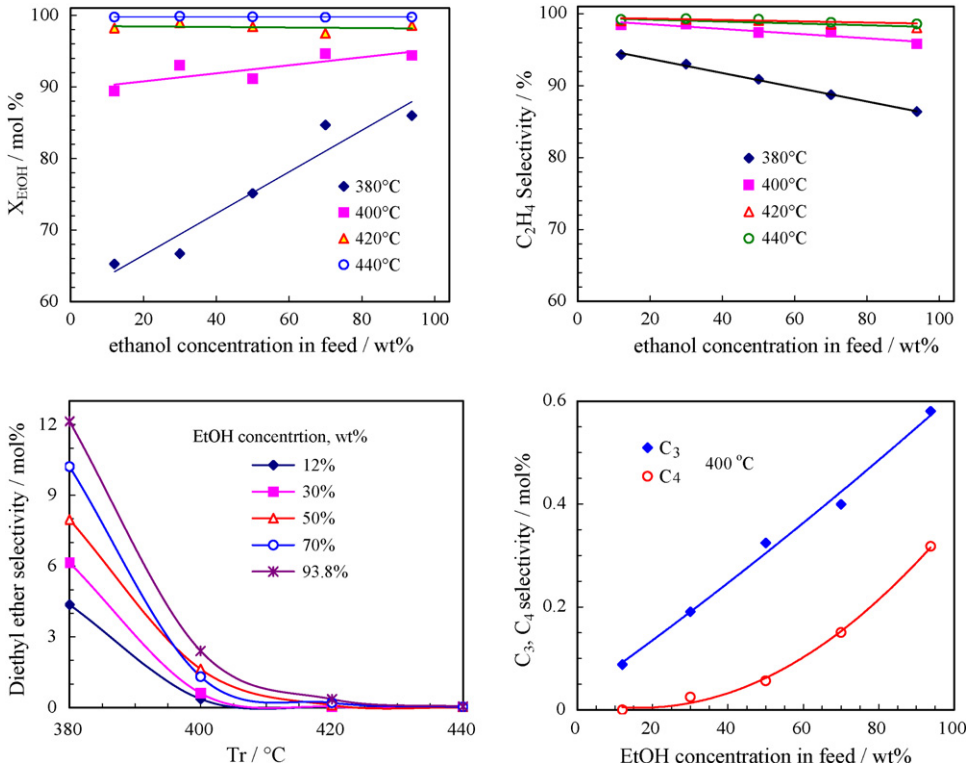


Fig. 9. Effect of feed composition; 10 wt% Ti/γ-$Al_2O_3$ catalyst, LHSV = 39 $h^{-1}$, and $p$ = 110–134 kPa.

### 3.3.3. *Effect of ethanol concentration on conversion and selectivity*

The concentration of bioethanol from fermentation synthesis is about 10 wt%, which contains large amount of water. In order to simplify the condensation process of bioethanol, it is necessary to develop processing techniques with flexibilities, in other words, to take the effect of water in ethanol solution on conversions and selectivities into account. The effects of the ethanol concentration on the ethanol conversion and the ethylene selectivity over 10 wt% Ti/γ-$Al_2O_3$ catalyst are shown in Fig. 9 and Table 3.

In Fig. 9, at a given space velocity and a reaction temperature, the conversion of ethanol decreases with the decreasing concentration of ethanol in the feed, especially when the temperatures are lower than 380 °C. The selectivity of ethylene increases with decreasing ethanol concentration, while the selectivity of ethyl ether is on the contrary. This may be because L-acid shifts to B-acid more easily on γ-$Al_2O_3$ due to increased water concentration that leads to decreased alumina basicity and dehydration activities at the one hand. At the other hand, competitive adsorption of water and ethanol on the active sites of the catalyst surface as proposed in reference [4]. But if the reaction temperatures are higher than 420 °C, the effects of water concentration in feed on the conversion and the selectivity would be weak. At the reaction temperature of 440 °C, the ethanol conversion, the ethylene selectivity and the ethylene yield are higher than 99.7%, 98.6% and 98.3%, respectively. The results listed in Table 3 indicate that the ethylene concentrations in gaseous phase are higher than 99 mol%. Additionally, the selectivities of $C_3$ and $C_4$ also decrease quickly with decreasing ethanol concentrations. From the process and system engineering view, the energy saving should be taken into account, there exists an optimal ethanol concentration of 30–50 wt% in feed.

### 3.3.4. *Effect of calcination temperature*

The ethanol catalytic dehydration on alumina is through Lewis acid and base pairs, where aluminum with empty orbit

Table 3
Gaseous phase products under different ethanol concentrations of feed ($T$ = 440 °C and LHSV = 52 $h^{-1}$)

| EtOH (wt%) | $Q_{gas}$ (mL/min) | Composition in gaseous phase (mol%) | | | | | $X_{EtOH}$ (mol%) | $S_E$ (mol%) | $Y_E$ (g/($g_{cat}$ h)) |
|---|---|---|---|---|---|---|---|---|---|
| | | $C_2H_6$ | $C_2H_4$ | $C_3$ | $C_4$ | DEE | | | |
| 12 | 47 | 0.40 | 99.55 | 0.05 | 0 | 0 | 99.7 | 99.2 | 4.4 |
| 30 | 103 | 0.25 | 99.6 | 0.13 | 0.01 | 0 | 99.9 | 99.3 | 9.8 |
| 50 | 170 | 0.19 | 99.5 | 0.24 | 0.04 | 0 | 99.8 | 99.2 | 16.0 |
| 70 | 227 | 0.24 | 99.15 | 0.40 | 0.12 | 0.01 | 99.7 | 98.8 | 21.2 |
| 93.8 | 281 | 0.23 | 99.0 | 0.41 | 0.23 | 0.02 | 99.7 | 98.6 | 26.1 |

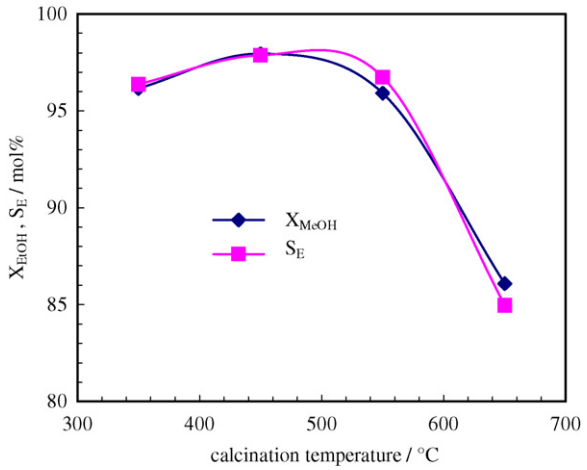


Fig. 10. The effect of calcination temperature; 93.8 wt% ethanol in feed, LHSV = 52 $h^{-1}$, $T_r$ = 420 °C, and $p$ = 110–130 kPa.

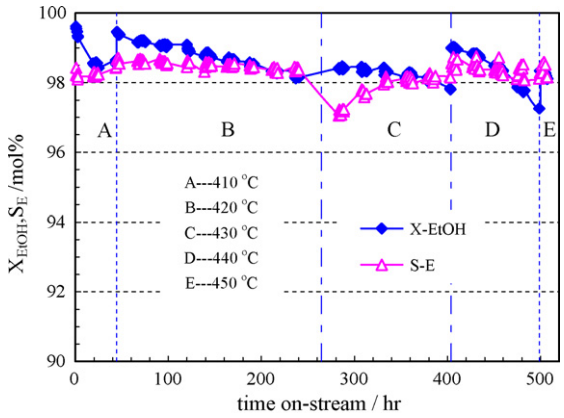


Fig. 11. The life-time of 10 wt% Ti/γ-$Al_2O_3$ catalyst. Reaction temperature: 410–450 °C, LHSV = 26 $h^{-1}$, and ethanol concentration: 93.8 wt%.

can act as an acid. The acid quantities and strengths on the surface have direct influence on the reaction stability: large amount of B-acid on surface can deactivate catalyst very quickly due to the adsorption of ethylene that can form polymers, and strong B-acid makes it difficult to control reaction temperatures at the early stage of the reaction process. Alumina only has Lewis acid sites, and the high calcination temperature leads to low concentrations of surface hydroxyl that affects the reaction through the carbon cation mechanism [33], so as to decrease catalyst activities. Fig. 10 shows the relationship of the conversion and the selectivity versus the calcination temperature of Ti/γ-$Al_2O_3$ catalysts prepared in different ways. The optimal calcination temperature are in the ranges of 400–500 °C.

### 3.3.5. Catalyst stability

Fig. 11 shows that the life-time testing curve at LHSV of 26 $h^{-1}$ and 93.8 wt% ethanol solution. The catalyst deactivates gradually, so the reaction temperature would be increased stepwise to maintain the ethanol conversion above 98%. In the first 400 h of the catalyst stability test, the conversion of ethanol is higher than 98% when reaction temperatures range from 410 to 430 °C. After 400 h, the catalyst deactivates very quickly, which illuminates that it is necessary to improve the stability of catalysts when the space velocity is 1–2 orders of magnitude higher than a conventional fixed bed reactor.

## 4. Conclusions

Highly active and relatively stable $TiO_2$/γ-$Al_2O_3$ catalysts are successfully incorporated into the microchannel plates in order to investigate the feasibility of intensification and miniaturization on the process of bioethanol-to-ethylene. Due to the small characteristic dimensions of the microchannel reactor, the effect of heat and mass transport is increased remarkably, and the trade-off scheme between the reaction temperature and the space velocity must be taken into consideration for the slow reactions. The experimental results demonstrate that the catalysts doped with 10 wt% $TiO_2$ have high ethanol conversions, ethylene selectivities and yields. The ethanol conversion of 99.96%, ethylene selectivity of 99.4% and ethylene yield of 26 g/($g_{cat}$ h) can be achieved. There exist optimal ethanol concentrations of 30–50 wt% and optimal calcination temperatures of 400–500 °C. The miniaturization of the bioethanol-to-ethylene process can be achieved with a microchannel reactor.

## Acknowledgements

We gratefully acknowledge the financial supports for this project from National Natural Science Foundation of China and China National Petroleum Corporation (nos. 20176057 and 20490208), 863 project (2006AA020101) and KIP program of Chinese Academy of Sciences (KSCX2-YW-G-003).

## References

[1] Y.L. Wu, S.J. Marwil, US Patent 4,234,752 (1980).
[2] T.K. Shioyama, US Patent 4,260,845 (1981).
[3] N.K. Kochar, R. Merims, A.S. Padia, CEP 77 (6) (1981) 66–70.
[4] S. Golay, R. Doepper, A. Renken, Chem. Eng. Sci. 54 (1999) 4469–4474.
[5] R.L. van Mao, T.M. Nguyen, G.P. Mclaughlin, Appl. Catal. 48 (1989) 265–277.
[6] X. Gao, I.E. Wachs, Catal. Today 51 (1999) 233–254.
[7] J.I. Di Cosimo, V.K. Díez, M. Xu, E. Iglesia, C.R. Apesteguíai, J. Catal. 178 (2) (1998) 499–510.
[8] T. Zaki, J. Colloid Interf. Sci. 284 (2005) 606–613.
[9] P. Berteau, B. Delmon, Catal. Today 5 (1989) 121–137.
[10] G.A. El-Shobaky, M.M. Doheim, A.M. Ghozza, H.A. El-Boohy, Mater. Lett. 57 (2002) 525–531.
[11] B.M. Abu-Zied, A.M. El-Awad, J. Mol. Catal. A 176 (2001) 227–246.
[12] B. Wan, S. Cheng, R.G. Anthony, A. Clearfield, J. Chem. Soc., Faraday Trans. 87 (9) (1991) 1419–1424.
[13] J. Haber, K. Pamin, L. Matachowski, B. Napruszewska, J. Poltowicz, J. Catal. 207 (2002) 296–306.
[14] E.A. El-Katatny, S.A. Halawy, M.A. Mohamed, M.I. Zaki, Appl. Catal. A 199 (2000) 83–92.
[15] M.M. Doheim, S.A. Hanafy, G.A. EI-Shobaky, Mater. Lett. 55 (2002) 304–311.
[16] K. Jähnisch, V. Hessel, H. Löwe, M. Baerns, Angew. Chem. Int. Ed. 43 (2004) 406.
[17] G. Kolb, V. Hessel, Chem. Eng. J. 98 (1–2) (2004) 1–38.
[18] G.W. Chen, Q. Yuan, J. Chem. Ind. Eng. (Chin.) 54 (4) (2003) 427–439.
[19] J. Kobayashi, Y. Mori, K. Okamoto, R. Akiyama, M. Ueno, T. Kitamori, S. Kobayashi, Science 304 (2004) 1305–1308.

[20] E.V. Rebrov, M.H.J.M. de Croon, J.C. Schouten, Catal. Today 69 (2001) 183–192.
[21] B. Cao, G.W. Chen, Q. Yuan, J. Chem. Ind. Eng. (Chin.) 55 (1) (2004) 42–47.
[22] J.D. Holladay, Y. Wang, E. Jones, Chem. Rev. 104 (2004) 4767–4790.
[23] G.W. Chen, Q. Yuan, H.Q. Li, S.L. Li, Chem. Eng. J. 101 (1–3) (2004) 101–106.
[24] S.L. Li, G.W. Chen, F.J. Jiao, H.Q. Li, Chin. J. Catal. 25 (12) (2004) 979–982.
[25] H. Ge, G.W. Chen, Q. Yuan, H.Q. Li, Catal. Today 110 (2005) 171–178.
[26] H. Kestenbaum, A.L. de Oliveira, W. Schmidt, F. Schüth, W. Ehrfeld, K. Gebauer, H. Löwe, T. Richter, D. Lebiedz, I. Untiedt, H. Züchner, Ind. Eng. Chem. Res. 41 (4) (2002) 710–719.
[27] R.M. Tiggelaar, P.W.H. Loeters, P. van Male, R.E. Oosterbroek, J.G.E. Gardeniers, M.H.J.M. de Croon, J.C. Schouten, M.C. Elwenspoek, A. van den Berg, Sens. Actuators A 112 (2004) 267–277.
[28] G.W. Chen, S.L. Li, Q. Yuan, Catal. Today 120 (2007) 63–70.
[29] M.R. Basila, T.R. Kantner, K.H. Rhee, J. Phys. Chem. 68 (1964) 3197–3203.
[30] K. Tanabe, Solid Acids and Bases – Their catalytic Properties, (in Chinese, Translated by Junsheng Zhao, Jiayu Zhang), Chem. Ind. Press, Beijing, 1979.
[31] E. Rodenas, T. Yamaguchi, H. Hattori, K. Tanabe, J. Catal. 69 (1981) 434–444.
[32] H. Arai, J. Take, Y. Saito, Y. Yoneda, J. Catal. 9 (1967) 146–153.
[33] V. Bosáček, V. Patzelová, Č. Hýbl, Z. Tvarůžková, J. Catal. 36 (3) (1975) 371–378.